Available online at www.sciencedirect.com
ScienceDirect
Trans. Nonferrous Met. Soc. China 33(2023) 3054−3066
Transactions of Nonferrous Metals Society of China
www.tnmsc.cn

Oxidation behavior and intermetallic compound growth dynamics of SAC305/Cu solder joints under rapid thermal shock

Ming WU[1], Shan-lin WANG[1], Li-meng YIN[2], Yu-hua CHEN[1], Min HONG[1], Wen-jun SUN[1], Zong-xiang YAO[2], Jia-ming NI[1], Peng LU[3], Ti-ming ZHANG[1], Ji-lin XIE[1]

1. Jiangxi Key Laboratory of Forming and Joining Technology for Aerospace Components, Nanchang Hangkong University, Nanchang 330063, China;
2. School of Metallurgy and Materials Engineering, Chongqing University of Science and Technology, Chongqing 401331, China;
3. Jiangxi MTC Optronics Co., Ltd., Nanchang 330006, China

Received 23 March 2022; accepted 13 July 2022

Abstract: Oxidation behavior of SAC305/Cu solder joints and kinetics of intermetallic compound (IMC) growth were investigated using an electromagnetic induction heating device. The results show that the solder joint undergoes oxidation when subjected to rapid thermal shock. The oxidation behavior of the solder joint itself is the main factor, which is exacerbated by the presence of the internal Cu_6Sn_5 IMC. The growth of the Cu_6Sn_5 layer is controlled by grain boundary diffusion, while that of the Cu_3Sn layer is controlled by bulk diffusion. The dissolved Cu of the substrate diffuses mainly into the interfacial IMC and the interior of the solder. Under rapid thermal shock, the shear strength of the solder joint decreases substantially, by 49.2% after 72 h. The fracture mechanism changes from ductile fracture to mixed tough−brittle fracture and finally, to brittle fracture.

Key words: induction heating; oxide film; SAC305; intermetallic compound; shear strength

1 Introduction

Earlier, SnPb solder, particularly Sn63Pb37, was among the most popular materials for soldering electronic components due to its excellent properties and low cost [1,2]. However, Pb is hazardous to human health and pollutes the environment, and the use of Pb-containing solders has been restricted or even eliminated in many countries [3,4]. Sn-based solders are sought after by many researchers due to their suitable melting interval and good performance, and among them, Sn3.0Ag0.5Cu (SAC305) solder is the most popular and is considered the best alternative to Sn63Pb37 solder [5,6].

When electronic equipment is in use, the solder joints become hot owing to various factors, which will have an impact on the thermal reliability of the solder joints [7]. The thermal reliability of solder joints depends mainly on two aspects: thermal aging and temperature cycling [8,9]. However, under thermal aging, the changes in the thermal load are small and take place over a very long time, making the duration of measurement quite long [8,10]. Compared to thermal aging, temperature cycling results in more destructive damage to the solder joint and a shorter inspection time due to the varied thermal stresses [11]. Depending on the rate of temperature change, temperature cycling is further divided into thermal cycling and thermal shock. Change in temperature

Corresponding author: Shan-lin WANG, Tel: +86-13755603426, E-mail: slwang70518@nchu.edu.cn;
Li-meng YIN, Tel: +86-15023730501, E-mail: yeenlm@cqust.edu.cn
DOI: 10.1016/S1003-6326(23)66317-4
1003-6326/© 2023 The Nonferrous Metals Society of China. Published by Elsevier Ltd & Science Press

is not higher than 20 °C/min for thermal cycling and not lower than 30 °C/min for thermal shock [12].

LI et al [13] observed the coarsening of the solder joint grain and stress concentration at the interface after 2500 cycles at a temperature change rate of 10 °C/min. Many misoriented grain boundaries were created within the solder joint during cycling, leading to crack formation and expansion in the high-strain region [14]. ZHONG et al [15] found that the solder joint corners crack after 250 cycles at a temperature change rate of 33 °C/min. However, recrystallization could prevent the solder from cracking by consuming the initial crack energy, resulting in excellent crack resistance. When the temperature change rate is 34.6 °C/min, TIAN et al [16] found that the growth mechanism of the intermetallic compound (IMC) layers is controlled by grain boundary diffusion, while large temperature changes can cause stress concentrations to form early cracks and lead to a decrease in the tensile strength. The fracture mode changes from ductile to brittle.

However, as the packaging density of the electronic products increases, the internal heat flow density increases, and the internal solder joints of the components are subjected to drastic changes in temperature. Typical conventional temperature cycle tests only have a small number of cycles and do not truly reflect the thermal effects of high power insulated-gate bipolar transistor (IGBT) devices and light-emitting diodes (LEDs) during reciprocal on/off and fast pulses. Therefore, a technique for repeated heating and cooling in a short time is needed to simulate the cyclic temperature loading [17].

Electromagnetic induction heating directly heats the metal using the eddy current effect and has high heating speeds and low consumption. Adopting such a heat source can reduce the test time. CHEN et al [18] verified the feasibility of electromagnetic induction heating to generate thermal shock that can result in rapid temperature changes in the solder joints compared to conventional methods, thus improving the testing efficiency. TIAN et al [19] compared the effects of electromagnetic induction thermal shock and conventional thermal shock on solder joints and found that cracks appeared on the top and sides of the solder joint surface as well as in the interior in the case of the former. Faster temperature changes result in shorter crack emergence time and faster crack expansion.

However, there are few studies on thermal shock generation using electromagnetic heating and there is a lack of systematic enquiry. Therefore, in this work, rapid thermal shock tests were performed by homemade electromagnetic induction heating equipment. The oxidation behavior of SAC305/Cu solder joints was investigated systematically, growth mechanism of the interfacial IMC layer was elucidated, and dissolution behavior of the Cu substrate was analyzed. In addition, the change in the fracture mode was determined by the analysis of the fracture surface. It is beneficial to improving the reliability of SAC305 solder joints under high frequency induction heating.

2 Experimental

2.1 Solder joint preparation

In this study, Sn3.0Ag0.5Cu (SAC305) ball grid array (BGA) with solder ball of 600 μm in diameter and copper-plated printed circuit board (PCB) pads (pad diameter of approximately 500 μm, and copper thickness of approximately 37 μm) were used in reflow soldering to form SAC305/Cu solder joints. The peak reflow temperature was 250 °C, the holding time above the liquid phase line was 95 s, and the temperature drop rate was 4 °C/s.

2.2 Thermal shock test

The solder joints were placed in a homemade thermal shock device for testing (Fig. 1). The device was equipped with a heating and cooling system. The high-frequency induction heating equipment (SP−40AB, SHUANGPING) was used as the heat source in heating system, and the heating rate was controlled by adjusting the heating current and time of the equipment. The equipment caused rapid heating of the working platform by electromagnetic induction generated by eddy currents, and then the solder joints were heated by solid−solid heat transfer. The cooling system was based on the principle of using circulating water to cool the working platform and the solder joints. The flow rate of the circulating water could be adjusted to control the cooling rate of the experiment. In this study, the heating current was 47.2 A, heating time was 10 s, and water flow speed was 1 m/s. The solder joints were subjected to a rapid thermal

shock test in the temperature range from 35 to 180 °C (Fig. 2). The heating time was 10 s, heating rate was 870 °C/min, cooling time was 124 s, and cooling rate was 70.2 °C/min. The high- and low-temperature dwell time was 5 s with a thermal shock cycle of 144 s, and total time was 72 h.

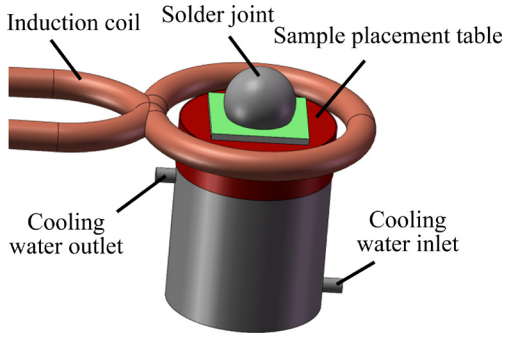

Fig. 1 Electromagnetic induction heating device

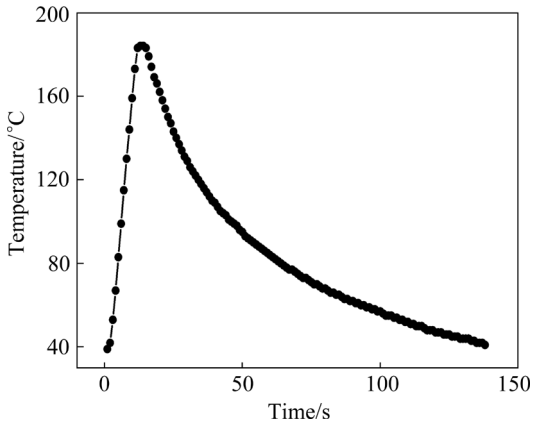

Fig. 2 Thermal shock temperature curve

2.3 Observation of morphology and interfacial microstructure

A scanning electron microscope (SEM SUPRA−55VP, ZEISS) equipped with a hot-electron X-ray energy dispersive spectrometer (EDS) was used to observe the surface morphology and the interfacial microstructure and to determine the phases in the interfacial region. Before observing the surface morphology, the solder joints were cleaned using C_2H_5OH solution. For solder joints with interfacial IMCs observation, the Sn was etched using HCl+HF+C_2H_5OH solution placed in ultrasonic waves for 5 min, followed by cleaning using C_2H_5OH solution. For the solder joints subjected to interfacial microstructure observation, they were first wrapped using epoxy resin, then sanded and polished using different sandpaper, and finally etched using HCl+C_2H_5OH solution for 15 s. Considering the irregular shape of the IMC layers, their thickness was measured digitally using Adobe Photoshop, while the average thickness of the IMC layers in the solder joint (x) was calculated by dividing the integrated area (A) by the length of the IMC layer (L), as shown in Eq. (1):

$$x=A/L \tag{1}$$

2.4 Shear test

The shear test was conducted using push−pull tester (MFM1200, TRY), where the shear speed was 400 μm/s and shear height was 40 μm. The shear strength was calculated according to Eq. (2), and five specimens were tested under each test condition to consider the average value:

$$\tau=\frac{1}{n_s}\sum_{i=1}^{n_s}\frac{F_i}{A_i} \tag{2}$$

where τ is the average shear strength of the solder joints (MPa), n_s is the number of solder joints, F_i is the maximum shear force of the solder joints (N), and A_i is the area of the solder joints (mm^2).

3 Results and discussion

3.1 Oxidation behavior of SAC305/Cu solder joints

Figure 3 shows the surface morphology of SAC305 solder joints under thermal shocks. From Fig. 3(a), before the thermal shock, the solder joints were well-formed with no obvious defects and the overall appearance was spherical. After 18 h of thermal shock (Fig. 3(b)), the surface of the solder joint was rough and distributed with voids, resulting in irregularly shaped solder joints. The size of the voids increased with time (Figs. 3(c, d)). At 54 h, the surface showed long strips of morphology that were detected to be Cu_6Sn_5 compounds. At 72 h, as shown in Fig. 3(e), the entire solder joint was covered by large, deep voids. This indicated that the rapid thermal shock changed the surface morphology of the solder joints and led to the development of defects. An EDS examination of the surface of the solder joint at 72 h revealed the presence of oxygen in large quantities, which indicated the oxidation behavior of the solder joint during thermal shock, caused by the conversion of Sn to SnO_2. It is known that Sn is easily oxidized at high temperatures to form compounds dominated by SnO_2. CHEN et al [20] used XRD to confirm the conversion of Sn to SnO_2 on the surface of solder

joints during thermal fatigue tests.

The BGA solder balls that were not interconnected with the copper substrate were tested for the same duration and the morphology is shown in Fig. 4. The solder balls that were not subjected to the thermal shock test were well-formed with no obvious defects, which is consistent with Fig. 3(a), indicating that the reflow process does not affect the

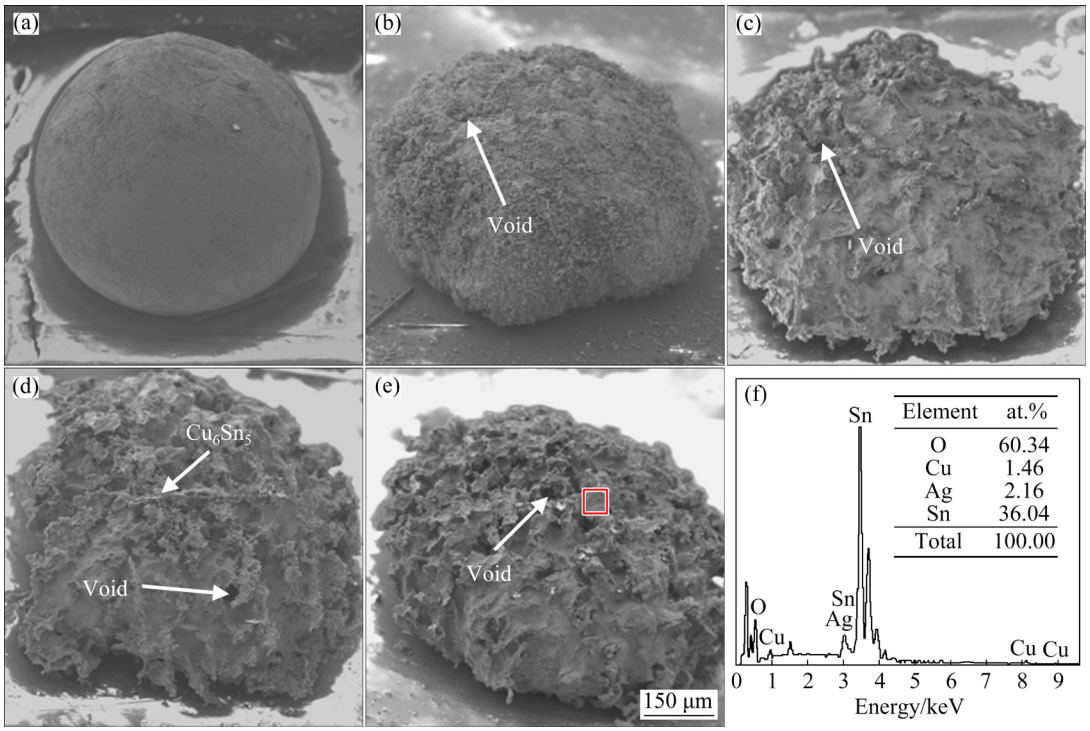

Fig. 3 Surface morphologies of solder joints under thermal shock for different time: (a) 0 h; (b) 18 h; (c) 36 h; (d) 54 h; (e, f) 72 h

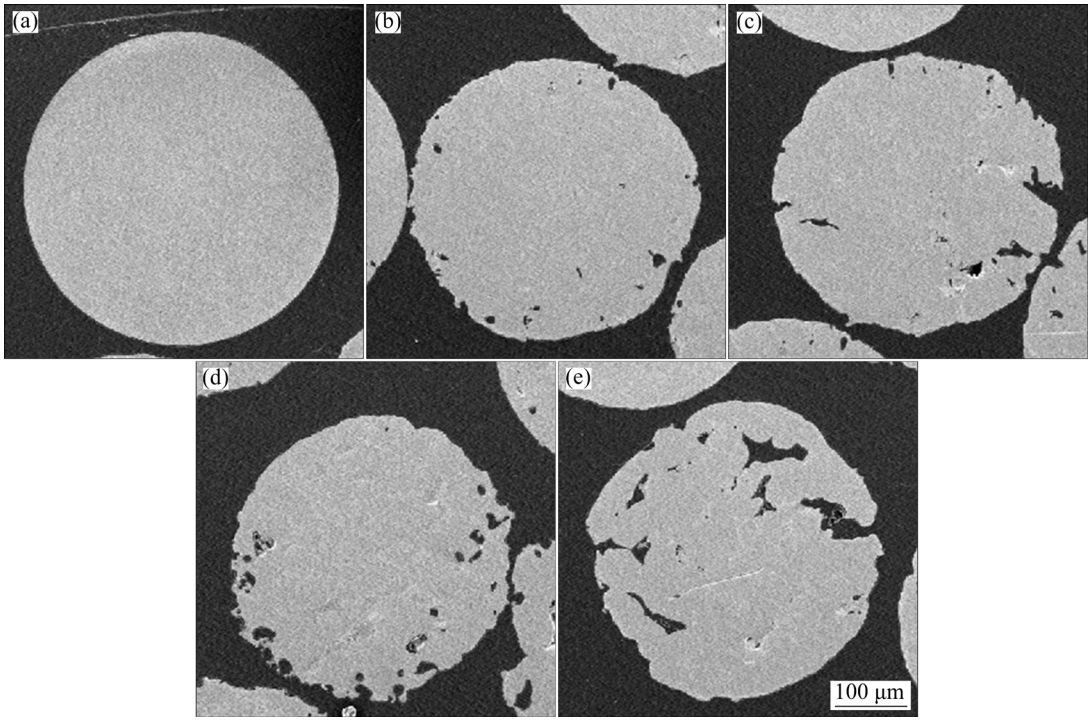

Fig. 4 Surface morphologies of BGA solder balls under thermal shock for different time: (a) 0 h; (b) 18 h; (c) 36 h; (d) 54 h; (e) 72 h

surface morphology of the solder joints. After 18 h of thermal shock (Fig. 4(b)), the edge of the solder ball started becoming irregular with the appearance of voids and cracks. As the thermal shock duration increased (Figs. 4(c, d)), the number of voids inside the solder ball increased and the cracks expanded to the interior, forming long and deep transverse cracks. As shown in Fig. 4(e), the voids inside the solder balls occupied a large proportion of the ball volume at 72 h, and the voids reached 90 μm at the longest point. This indicated that the oxidation behavior of the BGA solder balls has a great impact on the surface morphology and reliability of the solder joints in a rapid thermal shock environment.

Figure 5 shows that the Sn in the solder joints was etched using an etching solution to expose the internal IMC. Figures 5(a−c) showed the presence of long IMCs inside the solder joints, which had hollow structures that grew from the substrate toward the solder ball. From the perspective of elemental conservation, Cu_6Sn_5 was generated by the reaction between Cu and Sn atoms. It can be judged that during the reflow process, many Cu atoms diffused from the substrate to react with the Sn atoms inside the solder. The bottom−up temperature gradient generated during the reflow process resulted in the extension of the Cu_6Sn_5 from the interface to the upper part of the solder joints. As the thermal shock time increased (Figs. 5(b, c)), some of the Cu_6Sn_5 expanded laterally and fragmentation occurred.

From Figs. 3−5, there are two factors that contribute to the macroscopic morphological transformation of the solder joints during thermal shock, namely, the oxidation behavior of the solder ball itself and the internal IMC of the solder joint. Sn is an easily oxidizable metal that produces a thin oxide film on the surface of the solder joint after reflow. According to the Pilling−Bedworth theory, the ability of oxide films to protect the metal substrate depends on the integrity of the metal oxide film [21]. The underlying principle is that the volume of metal oxide films generated during oxidation (V_1) is larger than the volume of metal consumed to generate these oxide films (V_m). The value of V_1/V_m is greater than 1, and this ratio is called the Pilling−Bedworth ratio (PBR) value (R), which is expressed as

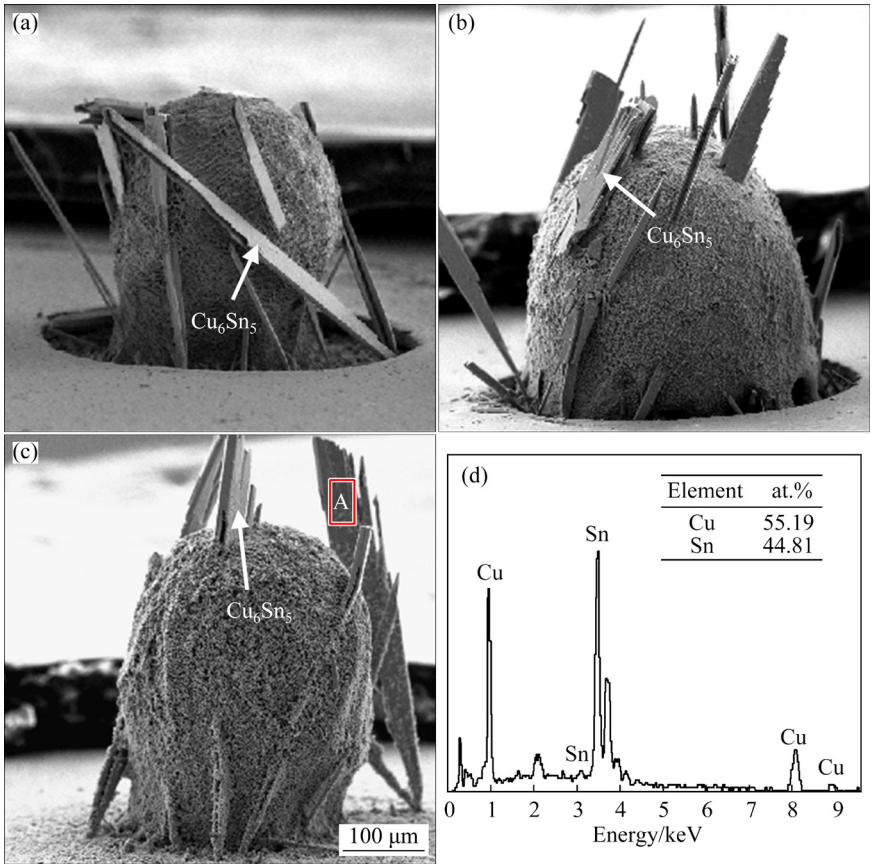

Fig. 5 Internal Cu_6Sn_5 morphologies of solder joints under thermal shock for different time (a−c) and EDS in Area A (d): (a) 0 h; (b) 18 h; (c) 54 h

$$R=\frac{V_1}{V_m}=\frac{M\rho_M}{NA\rho_1}=\frac{M\rho_M}{m\rho_1}>1 \quad (3)$$

where A is the relative molecular mass of the metal; M is the relative molecular mass of the metal oxide; N is the number of atoms of the metal in the metal oxide; m is the mass of the metal consumed to generate the oxide film; ρ_M and ρ_1 are the densities of the metal and the metal oxide.

Studies have shown that the oxide film is best protected when the PBR value is between 1 and 2. There is a thin layer of SnO_2 oxide film on the surface of the solder joints, and the PBR value of the SnO_2 oxide film at this time is 1.32 as calculated by Eq. (3). So, the oxidation resistance of the oxide film on the surface of the solder joints not subjected to thermal shock is better, which is the reason for the proper formation of the solder joints.

Figure 6 shows the oxidation behavior of the solder joints under thermal shock. The thermal expansion coefficient of the oxide films is usually lower than that of the metal substrate. Therefore, during the thermal shock cooling phase, the oxide film experiences compressive stresses. Conversely, it experiences tensile stresses during the heating phase, resulting in the presence of significant residual stresses within the oxide film. At some phase, the residual stress within the oxide film is released through cracks at the maximum curvature of the oxide film surface. When the interface strength of the oxide film metal is low enough, this can lead to oxide film peeling and voids formation [22]. During the thermal shock, due to the tip effect of stress concentration, areas subjected to the repeated action of tensile and compressive stress can be the first to crack. As time increases, the cracks continue to expand. On the one hand, the appearance of cracks quickly releases the stress within the film and leads to changes in the oxidation rate, and on the other hand, cracks act as channels for the fast diffusion of oxygen elements and thus play a direct role in promoting oxidation behavior.

The study indicates that the thermal expansion coefficient of SAC305 solder ball is 22.2×10^{-6} °C^{-1} and that of Cu_6Sn_5 is 16.3×10^{-6} °C^{-1}, and the difference in the thermal expansion coefficients is large [23]. During the thermal shock, the difference in thermal expansion coefficient causes the extrusion of the solder and Cu_6Sn_5, which further extends the cracks generated by the broken oxide film and provides more channels for the transfer of oxygen. Therefore, the oxidation behavior of the solder ball itself leads to the generation and extension of cracks during thermal shock, and the oxidation behavior is further improved by the difference in thermal expansion coefficients between the internal Cu_6Sn_5 and the solder.

The thermal stresses generated during cycling are

$$\sigma=\frac{C\alpha E\Delta T}{1-v} \quad (4)$$

where α is the coefficient of thermal expansion, E is the elastic modulus, ΔT is the cyclic temperature difference, C is a constant, and v is the Poisson's ratio.

It can be seen that, as the cyclic temperature increases, the thermal stresses generated in the cyclic process increase, thus increasing the damage to the material and the rate of formation and expansion of thermal shock fatigue cracks. During thermal shock, the rapid temperature transition is likely to cause a multi-axial stress state controlled by the tensile−compressive stress and creep fatigue, which can result in cracks, holes, and other defects.

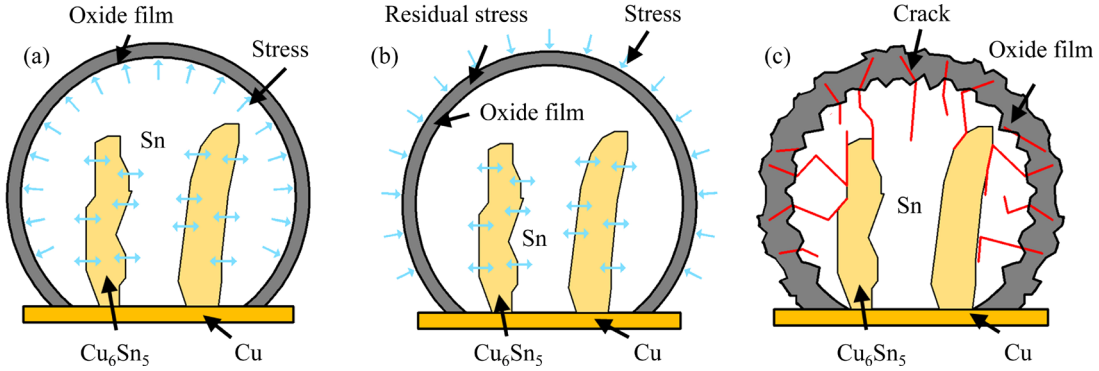

Fig. 6 Oxidation behavior of solder joints: (a) Heating phase; (b) Cooling phase; (c) After thermal shock

3.2 Evolution of interfacial IMC layer microstructure

Figure 7 shows microstructural transformation of the IMC layer of the SAC305 solder joints during thermal shock. Figure 7(a) shows that the interfacial IMC had single-layer structure before thermal shock, which was detected as Cu_6Sn_5 by EDS. This is due to the diffusion reaction of Cu and Sn atoms, which is a sign of metallurgical bonding between the solder balls and the substrate [24]. After 18 h of thermal shock (Fig. 7(b)), the interfacial IMC transformed into a double-layer structure with the addition of Cu_3Sn between Cu_6Sn_5 and Cu layer. Fine Ag_3Sn particles were also present. In addition, large pieces of Cu_6Sn_5 were observed near the interface, which was caused by the growth of Cu_6Sn_5 inside the solder joints. As shown in Figs. 7(c, d), the IMC layer became flat and the thickness increased with the thermal shock, especially Cu_3Sn. It was noteworthy that voids and cracks appeared at the interfacial IMC at 54 h, which might be due to the extension of the oxidation reaction to the interior of the solder joints, which further indicates that the oxidation reaction not only deteriorates the macroscopic morphology but also affects the internal microstructure.

Figure 8 shows the exposed IMC grains. It can be seen that the interfacial IMC layer consisted of a large number of grains, including Cu_6Sn_5 and Ag_3Sn grains, of which Cu_6Sn_5 grains accounted for the majority, and Ag_3Sn grains were sparsely distributed among the Cu_6Sn_5 grains. This is due to the presence of 3 wt.% Ag content in the SAC305 solder, and during reflow, Ag_3Sn grains reduce the surface energy between the interfacial IMC and the solder, which attach among the Cu6Sn5 grains [25]. As shown in Fig. 8(a), the Cu_6Sn_5 grains size were small after reflow and approximately 2.8 μm. At 18 h after the thermal shock (Fig. 8(b)), the grain size increased, with the average size reaching 5.5 μm. However, there were a large difference in size among the grains. As shown in Figs. 8(c, d), at 36 and 54 h, the grain size difference further increased. This is related to the growth model of the grains. As the large grains have longer grain boundaries, energy transfer from the surrounding

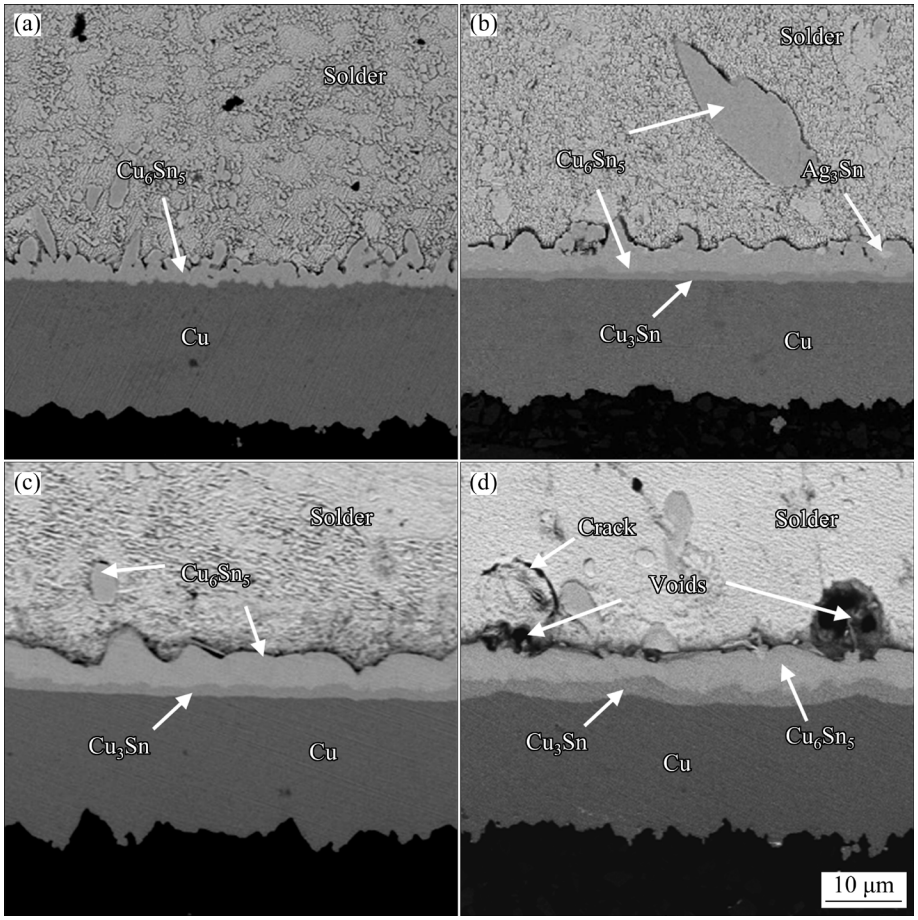

Fig. 7 Microstructure of IMC layer of SAC305 solder joints under thermal shock for different time: (a) 0 h; (b) 18 h; (c) 36 h; (d) 54 h

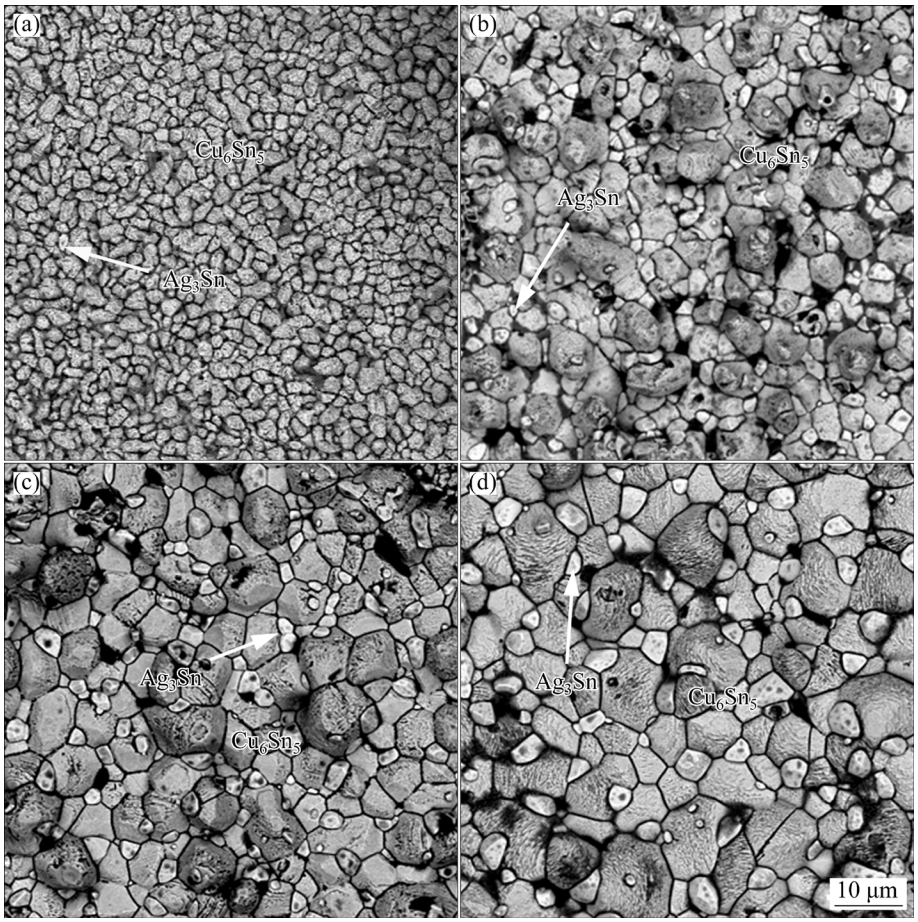

Fig. 8 Morphologies of IMC grains of SAC305 solder joints under thermal shock for different time: (a) 0 h; (b) 18 h; (c) 36 h; (d) 54 h

area for growth becomes easier, thus hindering energy acquisition by the small grains. In addition, the large grains annex the surrounding small grains in the surrounding area during the growth process, further hindering the growth of the small grains. When the Cu_6Sn_5 grains grow, Ag_3Sn particles grow alongside and attach themselves to the grain boundaries of the Cu_6Sn_5 grains.

3.3 Growth mechanism of interfacial IMC layer

Figure 9 shows the relationship between the thickness of the interfacial IMC layer and the thermal shock time. Each IMC layer at the interface grows in a parabolic manner, the growth rate slows down significantly, and the deceleration of the Cu_6Sn_5 layer is greater compared to Cu_3Sn layer. Each IMC layer at the interface is thin before the thermal shock, enabling the Sn and Cu to diffuse rapidly to form IMC. When the interfacial IMC layer thickens, the diffusion of Sn and Cu atoms is hindered [26,27]. This leads to a decrease in the growth rate of the interfacial IMC layers.

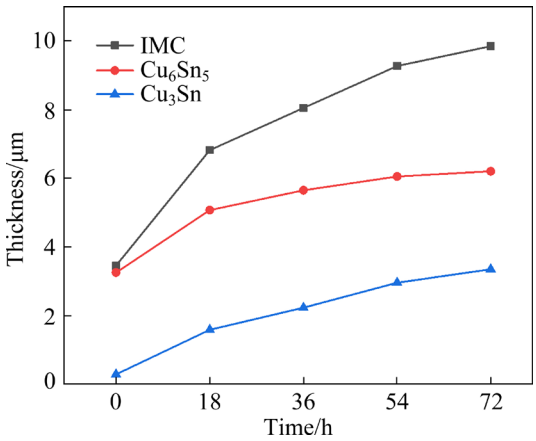

Fig. 9 IMC layer thickness under thermal shock

To elucidate the growth mechanism of the interfacial IMC layer, an empirical power-law equation can describe the growth mechanism of the interfacial IMC layer [28]:

$$x=x_0+kt^n \tag{5}$$

$$k=\frac{x-x_0}{t^n} \tag{6}$$

$$n=\frac{\ln(x-x_0)}{\ln t} \tag{7}$$

where x_0 is the thicknesses of the IMC layers (μm) before the thermal shock, k is the growth rate coefficient, t is the thermal shock time, and n is the time index.

The value of the time index n is a indicator of the growth mechanism of IMC layer [29,30]. If n is close to 1, the growth mechanism of IMC is considered to be controlled by interfacial reactions; if n is 1/2, the growth mechanism of IMC is considered to be controlled by bulk diffusion; similarly, if n is close to 1/3, the growth mechanism of the IMC is controlled by the grain boundary diffusion [31−33]. It is worth noting that during the thermal shock, since the temperature is variable, Vianco proposed an "effective growth time" to facilitate the calculation by approximating the thermal shock as an aging process, and the time was half of the total thermal shock time [34].

In this work, the values of the time index n and growth rate coefficient k were obtained by nonlinear regression analysis (Fig. 10 and Table 1).

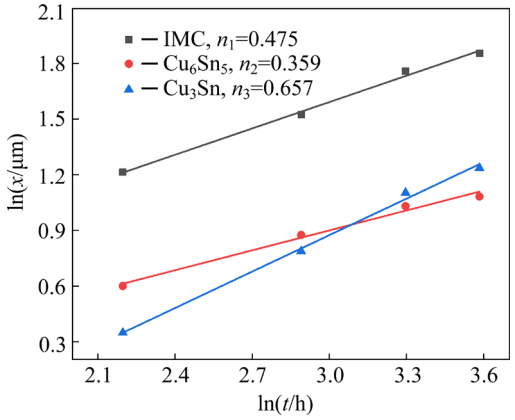

Fig. 10 SAC305 solder joint growth kinetic index fitting diagram

Table 1 IMC layer growth rate and growth mechanism of SAC305 solder joint

Layer	n	k/(μm·s^{-n})	R^2	IMC growth mechanism
IMC	0.475±0.023	1.180±0.054	0.992	Bulk diffusion
Cu_6Sn_5	0.359±0.028	0.821±0.007	0.997	Grain-boundary diffusion
Cu_3Sn	0.657±0.029	0.332±0.016	0.991	Bulk diffusion

The results show that the growth of the Cu_6Sn_5 layer is controlled primarily by grain boundary diffusion, and the growth of the Cu_3Sn layer is controlled primarily by bulk diffusion. The n value of the Cu_3Sn layer growth is greater than 0.5, indicating that other factors accelerate the growth of Cu_3Sn, and during thermal shock, when the thickness of Cu_6Sn_5 layer reaches a certain level, it prevents the diffusion of substrate Cu atoms into the solder, thus reacting with Cu_6Sn_5 at the IMC/Cu interface to generate Cu_3Sn. Overall, the IMC layer is controlled by bulk diffusion. This result is similar to thermal cycling, which indicates that the increase in temperature rate has less effect on the growth of IMC layers. The growth index is summarized in Table 1. The Cu_6Sn_5 layer has a faster growth rate compared to the Cu_3Sn layer during thermal shock, which is related to the fact that Cu_6Sn_5 has a lower activation energy.

3.4 Dissolution behavior of Cu substrate

Cu atoms from substrate diffusion flow to the interior of the solder and the IMC layer grows. Since the Cu content in the SAC305 solder does not reach saturation, it is assumed that the original Cu in the SAC305 solder does not participate in the interfacial IMC growth process. Thus, the Cu content in the interface IMC can be calculated from the IMC layer growth consumed by the thickness of the Cu substrate ($h_{\text{Cu-IMC}}$), so that the difference between the actual consumption of the Cu substrate thickness (h_{Cu}) and IMC growth consumed by the Cu substrate layer thickness ($h_{\text{Cu-IMC}}$) is the Cu substrate layers due to dissolution into the solder thickness ($h_{\text{Cu-solder}}$):

$$h_{\text{Cu-solder}}=h_{\text{Cu}}-h_{\text{Cu-IMC}} \tag{8}$$

According to the law of conservation of mass, there is

$$\rho_{\text{Cu}}h_{\text{Cu-IMC}}S_{\text{Cu}}=f_{\text{Cu}}\rho_{\text{IMC}}h_{\text{IMC}}S_{\text{IMC}} \tag{9}$$

where ρ_{Cu} is the density of Cu, ρ_{IMC} is the density of Cu−Sn IMC, f_{Cu} is the mass fraction of Cu in the Cu−Sn compound, S_{Cu} is the area of the Cu substrate consumption area, S_{IMC} is the area of Cu−Sn layer growth area, and h_{IMC} is the thickness of IMC layer. Since the size of BGA pads is fixed, it can be considered that the area of Cu substrate consumption (S_{Cu}) is the same as the area of Cu−Sn layer growth (S_{IMC}):

$$h_{\text{Cu-IMC}} = f_{\text{Cu}} \frac{\rho_{\text{IMC}}}{\rho_{\text{Cu}}} h_{\text{IMC}} \quad (10)$$

The density of Cu is 8.96 g/cm^3, the density of Cu_6Sn_5 is 8.28 g/cm^3 and the density of Cu_3Sn is 8.90 g/cm^3 [35]. Therefore, the thickness of Cu_6Sn_5 and Cu_3Sn need to be measured to calculate the Cu thickness consumed by the entire IMC layer.

The calculation results are shown in Fig. 11. From Fig. 11(a), it can be seen that most of the Cu enters the solder during reflow, and a small amount is used for the growth of the IMC layer. This is due to the high temperature at reflow and the violent reaction of the Sn and Cu atoms, which results in the generation of a large number of Cu−Sn compounds inside the solder joint and causes the appearance of Cu_6Sn_5 IMC inside the solder. The Cu atoms dissolved in the substrate during the thermal shock stage are mainly used for the growth of the IMC layer. Figure 11(b) shows that most of the Cu atoms consumed in the IMC layer during the reflow stage are used for the growth of Cu_6Sn_5 while a few are used for the growth of Cu_3Sn.

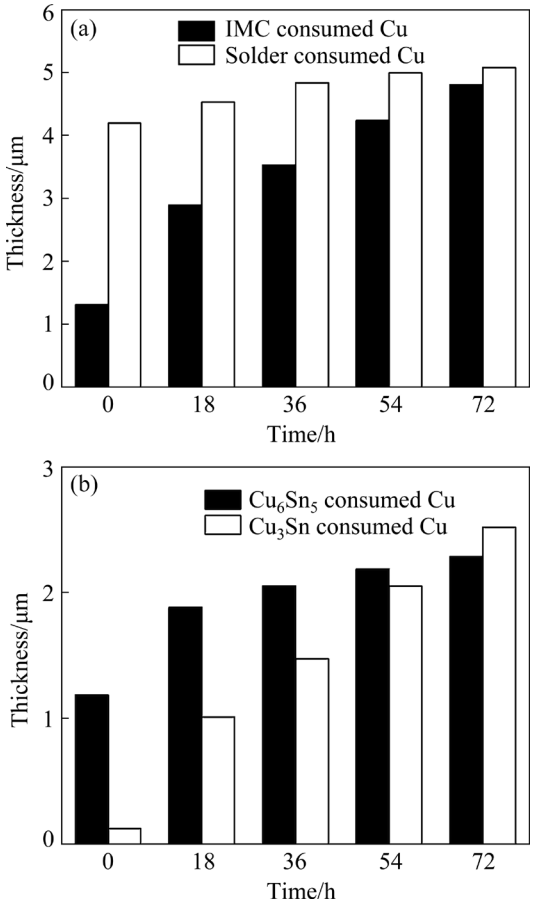

Fig. 11 Cu substrate dissolution thickness: (a) IMC layer and solder consumed Cu; (b) Cu_6Sn_5 layer and Cu_3Sn layer consumed Cu

Moreover, it takes three units of Cu to generate one unit of Cu_3Sn, and the Cu_3Sn layer is extremely thin at this time, which makes it difficult to observe the Cu_3Sn layer at the interface after reflow. As the thermal shock proceeds, the Cu thickness used for the growth of the Cu_6Sn_5 layer grows slowly. On the contrary, the Cu thickness used for the growth of the Cu_3Sn layer grows fast, which indicates that Cu_3Sn can grow rapidly when Cu_6Sn_5 reaches a certain thickness.

3.5 Shear strength and fracture behavior

Figure 12 shows the shear strength curves of the SAC305 solder joints at different thermal shock time. It can be seen that the shear strength of the solder joints decreased continuously with the extension of the thermal shock time. The strength of the solder joints before thermal shock was 54.55 MPa, and after 72 h, the strength decreased to 28.71 MPa, with a decline rate of 47.37%. This shows that rapid thermal shock significantly reduces the shear strength of the solder joint, thereby affecting the reliability of solder joints.

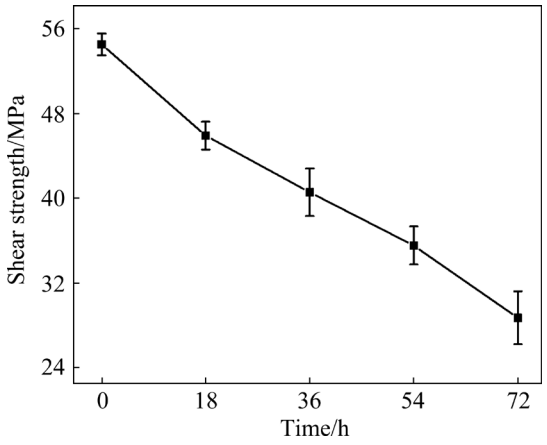

Fig. 12 Shear strength of SAC305 solder joints under thermal shock for different time

Figure 13 shows the fracture morphology of the SAC305 solder joints under thermal shock. From Fig. 13, it can be seen that solder joints changed from ductile fracture (Fig. 13(a)), which completely fractured inside the solder, to ductile−brittle fracture (Figs. 13(b−d)), which fractured in the solder as well as in the interfacial IMC layer, and finally to brittle fracture (Fig. 13(e)), which fractured in the interfacial IMC layer. Different fracture modes lead to different shear strengths as the solder-controlled ductile fracture has a high

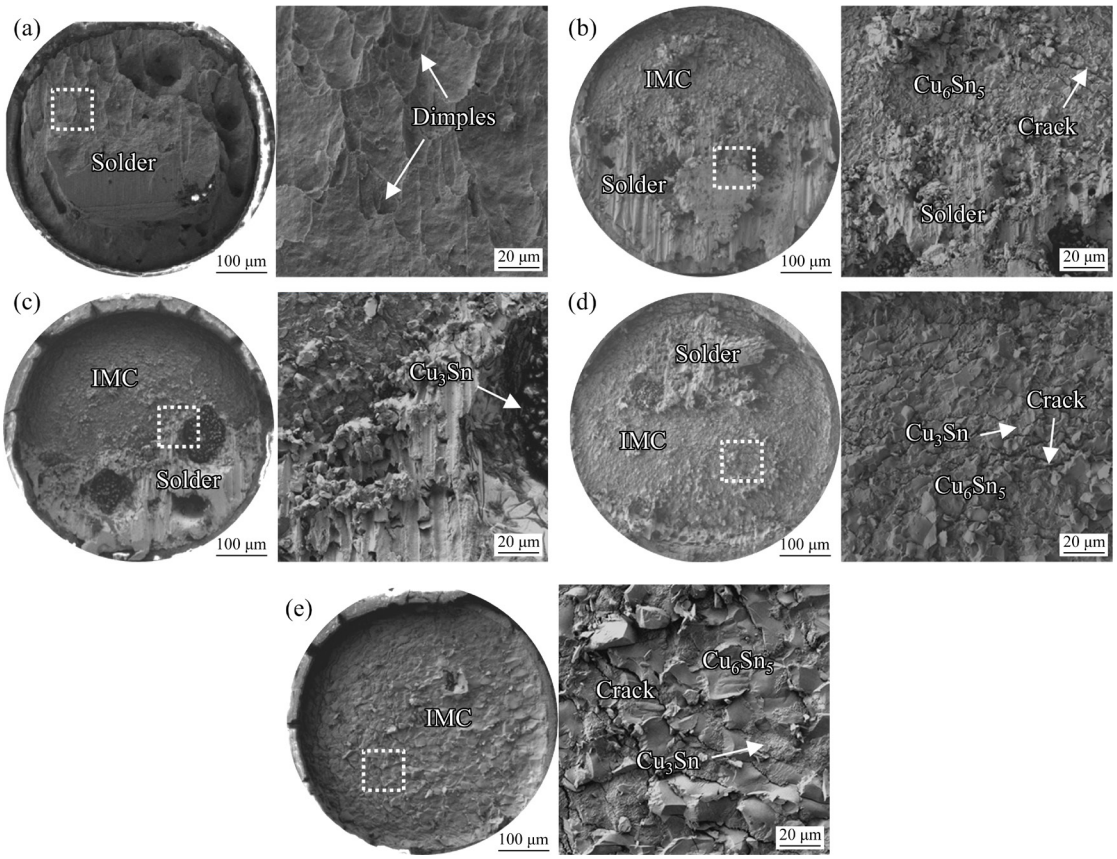

Fig. 13 Fracture surface morphologies of SAC305 solder joints under thermal shock for different time: (a) 0 h; (b) 18 h; (c) 36 h; (d) 54 h; (e) 72 h

shear strength; the brittle fracture controlled by the interface IMC layer has less strength in shear due to the brittleness of its own IMC layer; the mixed tough−brittle fracture is in between, mainly controlled by both the solder and the IMC layer. In addition, the shear stress and the brittle nature of the IMC layer during shear lead to cracks initiation at the edges of the solder joint which expand to the inside, further reducing the strength of the solder joint and resulting in a continuous decline in the shear strength of the solder joint during the change in the fracture mode.

4 Conclusions

(1) SAC305/Cu solder joints undergo the oxidation under rapid thermal shock, resulting in cracks and voids. The oxidation behavior of the solder balls themselves is the main factor, and the Cu_6Sn_5 IMC running through the inside of the solder joints promotes the oxidation behavior of the solder joint. The increase in thermal shock time leads to the expansion of cracks and voids.

(2) An empirical power-law relationship was used to elucidate the growth mechanism of the IMC layer during rapid thermal shock. The results show that the growth control mechanism for the IMC layer and Cu_3Sn layers is bulk diffusion, while the Cu_6Sn_5 layer is controlled by grain boundary diffusion. Compared with the Cu_3Sn layer, the Cu_6Sn_5 layer has a faster growth rate.

(3) The dissolution behavior of the Cu substrate was investigated. The substrate dissolved Cu is used for the growth of interfacial IMC and the interior of the solder. Most of the Cu is used for the growth of IMC layers and a small fraction goes inside the solder during thermal shock. The Cu dissolved in the substrate is mainly used for the growth of the Cu_6Sn_5 layer in the early stage of thermal shock, and mainly used for the growth of Cu_3Sn layer in the later stage.

(4) The shear strength of the solder joints decreased substantially during the thermal shock, by 49.2% after 72 h. The fracture mechanism changes from ductile fracture to mixed tough−brittle fracture and finally, to brittle fracture.

Acknowledgments

The authors are grateful for the financial support from the National Natural Science Foundation of China (Nos. 51965044, 52175288, 51865035).

References

[1] TIAN Ru-yu, HANG Chun-jin, TIAN Yan-hong, XU Ji-kai. Brittle fracture of Sn−37Pb solder joints induced by enhanced intermetallic compound growth under extreme temperature changes [J]. Journal of Materials Processing Technology, 2019, 268: 1−9.

[2] TUNTHAWIROON P, KANLAYASIRI K. Effects of Ag contents in Sn−*x*Ag lead-free solders on microstructure, corrosion behavior and interfacial reaction with Cu substrate [J]. Transactions of Nonferrous Metals Society of China, 2019, 29(8): 1696−1704.

[3] HAN Yong-dian, YANG Jia-hang, XU Lian-yong, JING Hong-yang, ZHAO Lei. Effect of transient current bonding on interfacial reaction in Ag-coated graphene Sn−Ag−Cu composite solder joints [J]. Transactions of Nonferrous Metals Society of China, 2021, 31(8): 2454−2467.

[4] EL-DALY A A, FAWZY A, MOHAMAD A Z, EL-TAHER A M. Microstructural evolution and tensile properties of Sn−5Sb solder alloy containing small amount of Ag and Cu [J]. Journal of Alloys and Compounds, 2011, 509: 4574−4582.

[5] KANLAYASIRI K, KONGCHAYASUKAWAT R. Property alterations of Sn−0.6Cu−0.05 Ni−Ge lead-free solder by Ag, Bi, In and Sb addition [J]. Transactions of Nonferrous Metals Society of China, 2018, 28(6): 1166−1175.

[6] AAMIR M, MUHAMMAD R, TOLOUEI-RAD M, GIASIN K, SILBERSCHMIDT V V. A review: Microstructure and properties of tin−silver−copper lead-free solder series for the applications of electronics [J]. Soldering & Surface Mount Technology, 2019, 32: 115−126.

[7] CHEN Guang, PENG Hao, SILBERSCHMIDT V V, CHAN Y C, LIU Chang-qing, WU Feng-shun. Performance of Sn−3.0Ag−0.5Cu composite solder with TiC reinforcement: Physical properties, solderability and microstructural evolution under isothermal ageing [J]. Journal of Alloys and Compounds, 2016, 685: 680−689.

[8] ZHANG Liang, XUE Song-bai, ZENG Guang, GAO Li-li, YE Huan. Interface reaction between SnAgCu/SnAgCuCe solders and Cu substrate subjected to thermal cycling and isothermal aging [J]. Journal of Alloys and Compounds, 2012, 510: 38−45.

[9] ZHOU Q, ZHOU B, LEE T K, BIELER T. Microstructural evolution of SAC305 solder joints in wafer level chip-scale packaging (WLCSP) with continuous and interrupted accelerated thermal cycling [J]. Journal of Electronic Materials, 2016, 45(6): 3013−3024.

[10] LIN Fei, BI Wen-zhen, JU Guo-kui, WANG Wu-rong, WEI Xi-cheng. Evolution of Ag_3Sn at Sn−3.0Ag−0.3Cu−0.05Cr/Cu joint interfaces during thermal aging [J]. Journal of Alloys and Compounds, 2011, 509: 6666−6672.

[11] AHSAN M A, HASAN K, FAHIM A, SUHLING J C, LALL P. Effect of different thermal cycling profiles on the mechanical behavior of SAC305 lead free solder [C]//19th IEEE Intersociety Conference on Thermal and Thermomechanical Phenomena in Electronic Systems (ITherm). IEEE, 2020: 1170−1179.

[12] LALL P, BHAT C, HANDE M, MORE V, VAIDYA R, GOEBEL K. Prognostication of residual life and latent damage assessment in lead-free electronics under thermomechanical loads [J]. IEEE Transactions on Industrial Electronics. 2011, 58(7): 2605−2616.

[13] LI Qi-hai, LI Cai-fu, ZHANG Wei, CHEN Wei-wei, LIU Zhi-quan. Microstructural evolution and failure mechanism of 62Sn36Pb2Ag/Cu solder joint during thermal cycling [J]. Microelectronics Reliability, 2019, 99: 12−18.

[14] LIBOT J B, ALEXIS J, DALVERNY O, ARNAUD L, DULONDEL F. Microstructural evolutions of Sn−3.0Ag−0.5Cu solder joints during thermal cycling [J]. Microelectronics Reliability, 2018, 83: 64−76.

[15] ZHONG Ying, LIU WEI, WANG Chun-qing, ZHAO Xiu-juan, CAERS J F J M. The influence of strengthening and recrystallization to the cracking behavior of Ni, Sb, Bi alloyed SnAgCu solder during thermal cycling [J]. Materials Science and Engineering A, 2016, 652: 264−270.

[16] TIAN Ru-yu, HANG Chun-jin, TIAN Yan-hong, ZHAO Li-you. Growth behavior of intermetallic compounds and early formation of cracks in Sn−3Ag−0.5Cu solder joints under extreme temperature thermal shock [J]. Materials Science and Engineering A, 2017, 709: 125−133.

[17] WU K C, LIN S Y, HUNG T Y, CHIANG K N. Reliability assessment of packaging solder joints under different thermal cycle loading rates [J]. IEEE Transactions on Device and Materials Reliability, 2015, 15(3): 437−442.

[18] CHEN J B, LI C, WU Y P. Study on rapid thermal cycling by inducted heating for microstructure of single SnAgCu solder joint [J]. Science and Technology of Welding and Joining, 2013, 17(3): 237−243.

[19] TIAN Mi-zhe, GAN Gui-sheng, CAO Hua-dong, YANG Dong-hua, JIANG Liu-jie, XIA Da-quan, SUN Peng-fei, LIU Xin, WU Yi-ping. Effect of rapid thermal fatigue on microstructure and properties of Sn3.0Ag0.5Cu/Cu solder bumps [C]//21st International Conference on Electronic Packaging Technology (ICEPT). IEEE, 2020: 1−4.

[20] CHEN Ji-bing, YIN Yan-fang, YE Jian-ping, WU Yi-ping. Investigation on fatigue behavior of single SnAgCu/SnPb solder joint by rapid thermal cycling [J]. Soldering & Surface Mount Technology, 2015, 27(2): 76−83.

[21] HA S H, YOON Y O, KIM B H, LIM H K, LEE T W, LIM S H, KIM S K. Pilling−Bedworth ratio approach to surface oxidation of Al−Mg alloys containing Al_2Ca and its experimental verification [J]. Science of Advanced Materials, 2018, 10(5): 697−700.

[22] LIU Wei-hua, ZUO Yu, CHEN Sheng-li, ZHAO Xu-hui, ZHAO Jing-mao. The effects of sealing on cracking tendency of anodic films on 2024 aluminum alloy after heating up to 300 °C [J]. Surface and Coatings Technology, 2009, 203(9): 1244−1251.

[23] ZHONG Ying, AN Rong, WANG Chun-qing, ZHENG Zhen,

LIU Zhi-quan, LIU Chin-hung, LI Cai-fu, KIM T K, JIN S H. Low temperature sintering Cu_6Sn_5 nanoparticles for superplastic and super-uniform high temperature circuit interconnections [J]. Small, 2015, 11(33): 4097−4103.

[24] DEPIVER J, MALLIK S, AMALU D E H. Effective solder for improved thermo-mechanical reliability of solder joints in ball grid array (BGA) soldered on printed circuit board (PCB) [J]. Journal of Electronic Materials, 2021, 50(1): 263−282.

[25] HUANG M L, LOEHER T, OSTMANN A, REICHL H. Role of Cu in dissolution kinetics of Cu metallization in molten Sn-based solders [J]. Applied Physics Letters, 2005, 86(18): 7257−7904.

[26] SHEN J, CHAN Y C, LIU S Y. Growth mechanism of Ni_3Sn_4 in a Sn/Ni liquid/solid interfacial reaction [J]. Acta Materialia, 2009, 57(17): 5196−5206.

[27] LI J F, AGYAKWA P A, JOHNSON C M. Interfacial reaction in Cu/Sn/Cu system during the transient liquid phase soldering process [J]. Acta Materialia, 2011, 59(3): 1198−1211.

[28] XIONG Ming-yue, ZHANG Liang. Interface reaction and intermetallic compound growth behavior of Sn−Ag−Cu lead-free solder joints on different substrates in electronic packaging [J]. Journal of Materials Science, 2019, 54(2): 1741−1768.

[29] LI Hai-long, AN Rong, WANG Chun-qing, JIANG Zhi. In situ quantitative study of microstructural evolution at the interface of Sn3.0Ag0.5Cu/Cu solder joint during solid state aging [J]. Journal of Alloys and Compounds, 2015, 634: 94−98.

[30] DENG X, PIOTROWSKI G, WILLIAMS J J, CHAWLA N. Influence of initial morphology and thickness of Cu_6Sn_5 and Cu_3Sn intermetallics on growth and evolution during thermal aging of Sn−Ag solder/Cu joints [J]. Journal of Electronic Materials, 2003, 32(12): 1403−1413.

[31] HUANG M L, YANG F. Size effect model on kinetics of interfacial reaction between Sn−*x*Ag−*y*Cu solders and Cu substrate [J]. Scientific Reports, 2014, 4(1): 1−9.

[32] BAO Ni-fa, HU Xiao-wu, LI Qing-lin, LI Shuang. Effect of Cu concentration on the interfacial reactions between Sn−*x*Cu solders and Cu substrate [J]. Materials Research Express, 2019, 6(7): 076310.

[33] KIM D G, JUNG S B. Interfacial reactions and growth kinetics for intermetallic compound layer between In−48Sn solder and bare Cu substrate [J]. Journal of Alloys and Compounds, 2005, 386: 151−156.

[34] VIANCO P T, STEPHENS J J, REJENT J A. Intermetallic compound layer development during the solid state thermal aging of 63Sn−37Pb solder/Au−Pt−Pd thick film couples [J]. IEEE Transactions on Components, Packaging, and Manufacturing Technology: Part A, 1997, 20(4): 478−490.

[35] BOETTINGER W J, JOHNSON C E, BENDERSKY L A, MOON K W, WILLIAMS M E, STAFFORD G R. Whisker and Hillock formation on Sn, Sn−Cu and Sn−Pb electrodeposits [J]. Acta Materialia, 2005, 53(19): 5033−5050.

快速热冲击下 SAC305/Cu 焊点氧化行为与金属间化合物生长动力学

吴 鸣[1]，王善林[1]，尹立孟[2]，陈玉华[1]，洪 敏[1]，孙文君[1]，
姚宗湘[2]，倪佳明[1]，卢 鹏[3]，张体明[1]，谢吉林[1]

1. 南昌航空大学 江西省航空构件成形与连接重点实验室，南昌 330036；
2. 重庆科技学院 冶金与材料工程学院，重庆 401331；
3. 江西兆驰光电有限公司，南昌 330006

摘 要：通过电磁感应加热装置，研究 SAC305/Cu 焊点氧化行为和界面金属间化合物(IMC)生长动力学。结果表明，快速热冲击下焊点自身氧化行为是主要因素，内部的 Cu_6Sn_5 IMC 会加剧焊点的氧化。Cu_6Sn_5 层的生长由晶界扩散控制，Cu_3Sn 层的生长则由体扩散控制。基底溶解的 Cu 原子主要扩散到界面 IMC 和焊料的内部。在快速热冲击下，焊点剪切强度大幅度降低，72 h 后下降 49.2%。断裂机制由韧性断裂向韧脆性混合断裂转变，最终转变为脆性断裂。

关键词：感应加热；氧化膜；SAC305；金属间化合物；剪切强度

(Edited by Bing YANG)